2017

Optical and Electronic Investigation of Hydrogen-Bonded Organic Semiconductor Quinacridone

Michael V. Arnold
University of Vermont

Optical and Electronic Investigation of Hydrogen-Bonded Organic Semiconductor Quinacridone

A Thesis Presented

by

Michael Arnold

to

The Faculty of the College of Arts and Sciences

of

The University of Vermont

In Partial Fulfillment of the Requirements
for the Degree of Bachelor of Science
Specializing in Physics

May, 2017

Defense Date: May 1, 2017
Thesis Examination Committee:

Matthew White, Advisor
Madalina Furis, Advisor
Severin Schneebeli, Chairperson

Abstract

The viability of solar power is currently limited by the expense and processing limitations of existing inorganic technology. Organic semiconductors offer the possibility of scalable, economically appealing solar cell technologies. Quinacridone is a promising material which has recently been shown to have electronic properties comparable to the fully π-conjugated, but structurally similar pentacene, while remaining chemically stable in air. In order to better understand the potential of quinacridone as a candidate material for viable, next generation solar cells we have fabricated a number of thin-film samples and device structures and characterized them by a suite of optical and electronic tests.

Absorbance and temperature-dependent photoluminescence studies were used as a probe to investigate the electronic states of vapor deposited quinacridone thin films, finding exciton binding energies consistent with excitonic states delocalized across several molecules. Impedance spectroscopy measurements were used to measure the temperature-dependent photoconductivity of Gold : Quinacridone : Gold MSM structures, finding that quinacridone is almost an order of magnitude more conductive under laser illumination. Diode structures of ITO:PEDOT:Quinacridone:Al were fabricated to measure the IV characteristics under light and dark conditions, as well as the transient photocurrent and photovoltage. These studies confirmed that the light current generation of the diodes was not limited by charge transfer state lifetimes, as charge extraction occurs on a much faster time scale. However, we found that the low mobility of our quinacridone thin films, caused by their low crystalline order, decreased the probability of exciton dissociation, limiting the production of usable power.

Acknowledgements

I would first like to thank my advisors Professor White and Professor Furis who have invested countless hours in answering my questions over the past three years. Your guidance and encouragement have enriched my academic experience and offered me opportunities I could hardly imagine.

Thanks to my professors in the physics department, particularly Professor Del Maestro, who has taught me the ropes of computational physics, which has been invaluable for this thesis and in my academic life, and Professor Spartalian, who encouraged my experimental curiosity and showed me the value of an analysis done right. Thanks to Professor Clougherty, whose clarity in instruction has been instrumental in my understanding of physics, and to Professor Headrick, who still hasn't banned me from his labs. Thanks to all of the graduate students who have taken the time to help me over the years, especially Kim Hua, Jing Wan, and Yang Li, who have made many of the measurements in this thesis possible.

Thanks to the Physics Department Crowell Award and the Office of Undergraduate Research SURF and Mini Grant, which have supported every project I've proposed.

Finally, I'm grateful to my parents and siblings, who have always nurtured my curiosity and given me the tools to explore, and to Summer who always pushes me to be better when I need it most.

Table of Contents

List of Figures

List of Tables

Chapter 1

Introduction

1.1 Organic Semiconductors

Organic Semiconductors have been investigated as an alternative to more well-established inorganic semiconductors such as Silicon (Si) and Gallium Arsenide (GaAs). There are many applications of semiconductor technology, including photovoltaics (PV), light emitting diodes (LEDs), and field effect transistors (FET) for which organics could potentially compete with their inorganic predecessors. Even today organic LEDs (OLEDs) can be seen replacing older LED technologies in consumer TVs, demonstrating the rapid development and commercial viability of organic technology.

Advancement in photovoltaic technology offer the possibility of scalable, economically appealing solar cell technologies. The viability of solar power is currently limited by the expense and processing limitations of existing inorganic technology. Organic alternatives are hoped to cut to the cost of producing PV and increase production volume. Much of the foundational work in organic semiconductors has been done

with aromatic, small molecules like tetracene and pentacene [1], which have good electronic properties, such has high mobility, due to the delocalizing effects of full π-conjugation, but are chemically unstable in the presence of light and oxygen. Research into hydrogen-bonded semiconductors hopes to select molecules which retain the electronic properties for devices, while remaining chemically stable in air, a critical requirement for wide-scale adoption. Quinacridone is a promising material and recently researchers [2] have claimed it has among the best mobility and stability, when deposition techniques optimized.

The goal of this work is to better understand the potential of quinacridone as a candidate material for viable, next generation solar cells by fabricating a number of thin-film samples and device structures for characterization by a suite of optical and electronic tests.

1.2 Quinacridone: Air-Stable Hydrogen-Bonded, Organic Semiconductor

Quinacridone was chosen as a material of interest because of the strong similarity in molecular structure to pentacene. Looking at Figure 1.1, we see that while pentacene is fully π-conjugated, this conjugation is broken in quinacridone molecules by the carbonyl and amine groups, which has a localizing effect on π-electrons within the molecule. However, the addition of these groups causes intermolecular hydrogen bonding, which in turn changes the crystal packing structure from herringboned to planar, as shown in Figure 1.1. In the planar geometry, delocalization can occur along π stacking axis, increasing the rate of charge transfer between molecules. In

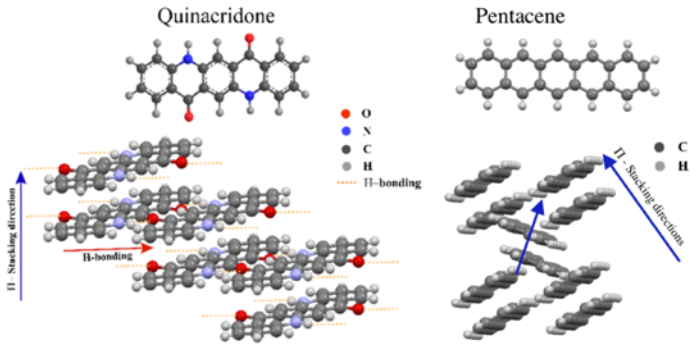

Figure 1.1: Molecular Structure and Crystal Packing of Quinacridone vs Pentacene

addition, the strength of hydrogen-bonds increase the crystalline order compared to weaker van der Waals intermolecular interactions of pentacene, which should lead to higher carrier mobility. This intermolecular delocalization could potentially lower the Coulombic binding energy of the excited electronic state: the exciton binding energy.

Chapter 2

Optical Characterization

Optical characterization allows us to probe the energy structure of semiconducting materials. For solar applications, we desire materials that absorb over a broad range of wavelengths, and materials with highly emissive photoluminescence. Broad absorbance offers the potential of harnessing more of the sun's energy, while highly emissive photoluminescence suggests that the fastest pathway for excited state relaxation is through radiative transitions, and thus less of the energy of the absorbed photons will be lost due to non-radiative processes. [**?**]

2.1 Sample Preparation and Measurement Procedure

To make samples, commercially available quinacridone was purified using our three-zone, vacuum sublimation furnace. Thin sapphire substrates were washed sequentially in ultrasonic baths of de-ionized water, and isopropanol. Approximately 100 nm

of quinacridone was vapor deposited on the sapphire substrate. The thickness of a sample evaporated in parallel was measured using a stylus profilometer. After viewing the resulting films under a linearly polarized microscope, we concluded the films were polycrystalline with sub-micron grain sizes.

For absorbance measurements samples were mounted on an optics table, where a monochromator is used to select a wavelength of light from a Xenon lamp, which is sent through an optical chopper, passes through the sample, where some of the light is absorbed, and the transmitted light is detected by a photodiode. The current signal from the photodiode is amplified by a lock-in amplifier, and matched to its respective wavelength by a Labview VI. The signal is corrected for the emission spectrum of the lamp, and the sensitivity spectrum of the photodiode.

For temperature dependent photoluminescence measurements, the samples were mounted in an optical cyrostat and excited using a 532 nm laser. The cyrostat temperature was varied incrementally from 4.3 K to 295 K. The emitted light passed through a beam splitter and optical filters to reduce the intensity of the laser light before entering the spectrometer. A labview VI was used to control the grating in the spectrometer to select the desired wavelength window to be recorded. The slit size was kept constant throughout the measurement, and the exposure time was varied from 1 second for low temperature measurements, to 2 seconds for higher temperature measurements. This factor was controlled for in post processing.

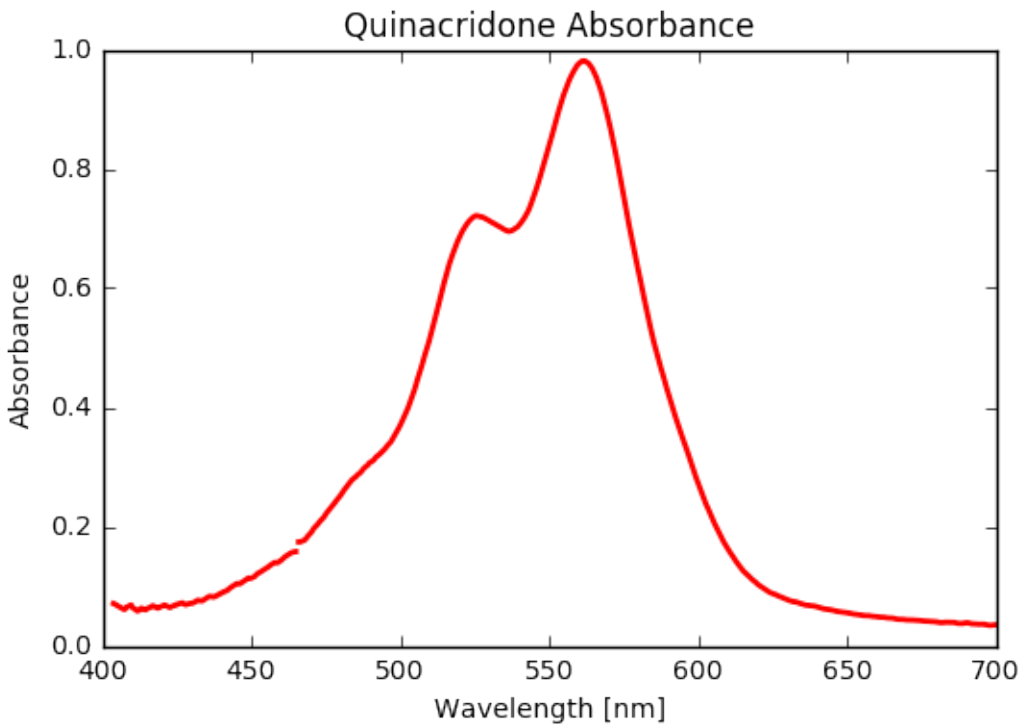

Figure 2.1: Quinacridone Absorbance as a Function of Wavelength

2.2 Absorbance

Absorbance measures the fraction of incident photons absorbed by a material as a function of wavelength. In the resulting plot, we see two peaks, at 525 nm and 561 nm. The absorbance spectrum was used to choose the 532 nm laser for the photoluminescence study, where absorbance is high. Additionally, there must be available electronic states for photons of this energy to be absorbed. For solar applications broad absorption peaks are desired with significant overlap with the solar spectrum.

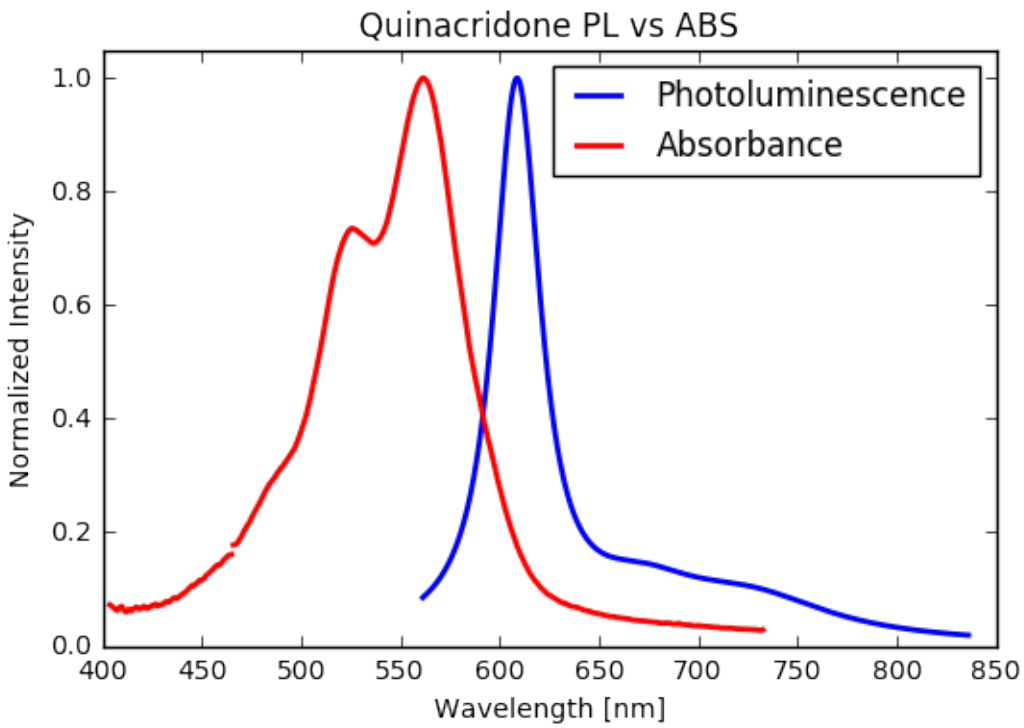

Figure 2.2: Quinacridone normalized Photoluminescence and Absorbance

2.3 Photoluminescence

Photoluminescence measurements count the number and wavelength of photons emitted when a sample is excited by an illumination source, in this case a focused 532 nm laser beam. As we vary the temperature, the line shape of the photoluminescence changes, reflecting the altered energy landscape of available states as the thermal energy is changed. Comparing the normalized room temperature PL and Absorbance in Figure 2.2 we see that the PL 0-0 peak has a much sharper onset from the high energy side, than the absorbance peak. This is likely caused by reabsorption of high energy photons which are emitted inside the bulk of the quinacridone film.

At low temperatures, the luminescence spectrum is dominated by a peak at 617 nm, suggesting an energy gap of 2.002 eV between the lowest available vibrational state of the excited electronic state and the relaxed state [3], because non-radiative relaxations (thermalization) occur on a much faster time-scale than radiative ones. This peak has been fitted with a slightly asymmetric guassian to model the steep onset at higher energies. A second, smaller peak is present at 638 nm, while a third, broader peak is present at 692 nm.

We see that as we raise the temperature, the 0-1 peak increases in intensity relative to the 0-0 peak, becoming a distinct shoulder at 35 K and 45 K, and becoming prominent at 70 K and 90 K.

Compared to a similar room temperature quinacridone thin film photoluminescence study reported by Glowacki et.al.[6], our study confirms a peak around 617 nm, but does not reproduce the broad mass extending to 800 nm, that they claimed was due to emission from dissociative states. This may result from different film deposition conditions.

The peaks were also fitted as a linear combination of Guassian features as shown in Figure 2.5, where the example of the 15 K measurement is shown.

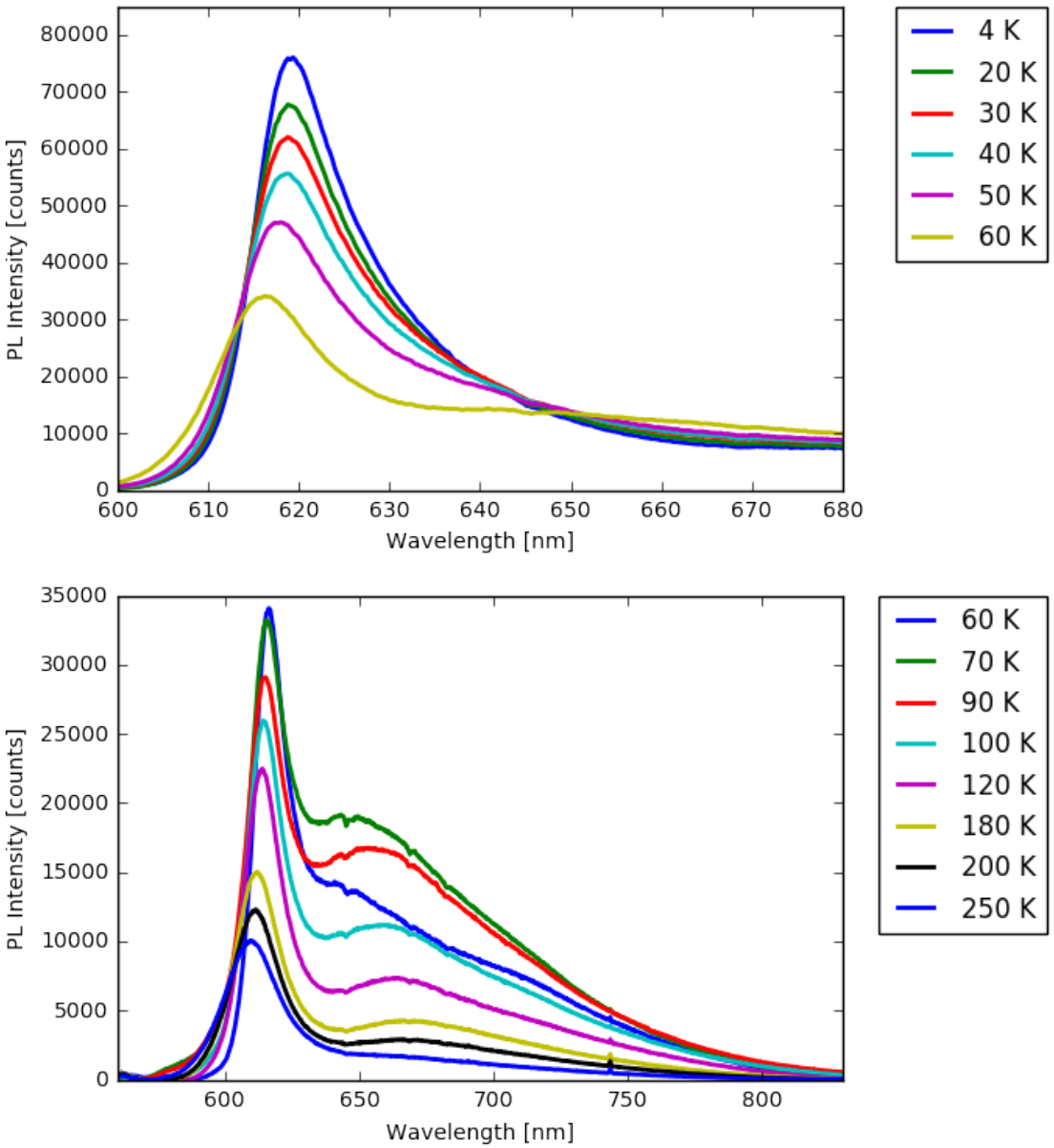

Figure 2.3: Quinacridone Temperature Dependent Photoluminescence

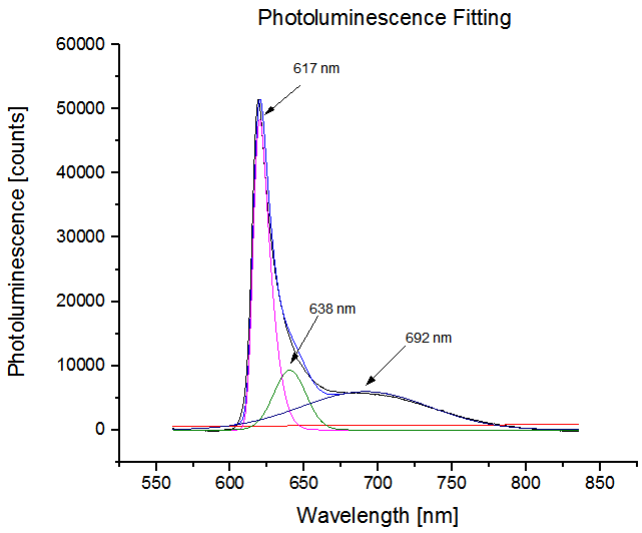

Figure 2.4: Quinacridone 15 K Fitting

2.4 Arrhenius Fitting and Binding Energy

To extract the binding energy from our temperature dependent data, we use the Arrhenius equation which relates the intensity of PL peaks to temperature:

$$I(T) = \frac{I_0}{1 + C\exp\left(\frac{E_b}{k_b T}\right)}$$

where, I(T) is the intensity of a feature at a given temperature I_0 is the intensity of the peak at the lowest temperature (4.3 K in our case), and E_b is the exciton binding energy. The intensity of a feature was found fitting the PL curve with 3 Gaussian peaks for each temperature, and integrating over the 0-0 peak, to find the total intensity resulting from that transition. Rearranging the Arrhenius equation,

we find that

$$ln(I(T)/I_0) = -\frac{E_b}{k_b T} + c$$

When $ln(I(T)/I_0)$ was plotted against inverse temperature and fitted with this equation, the exciton binding energy was found to be $E_b = 22$ meV.

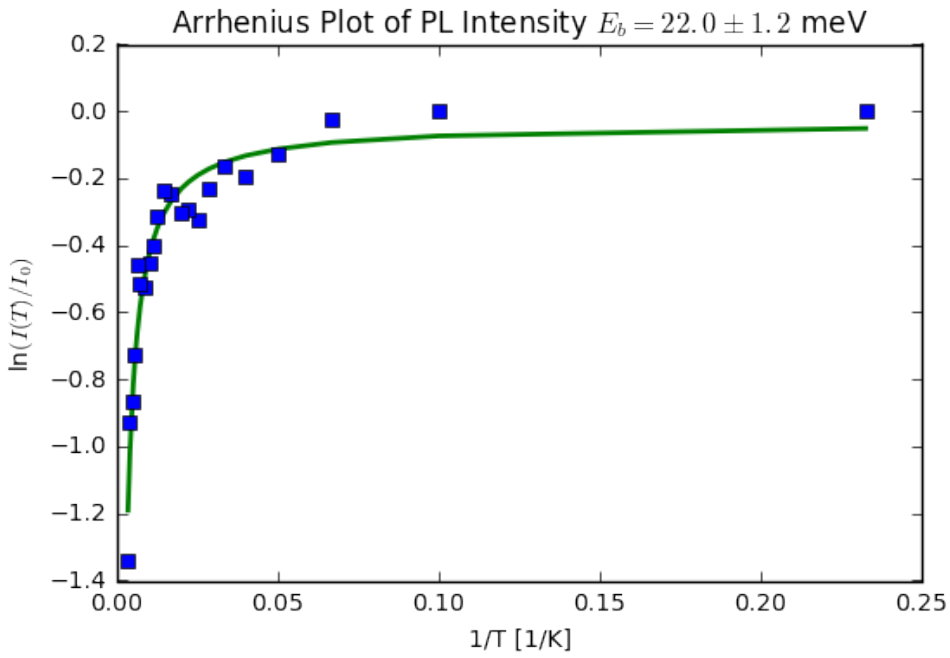

Figure 2.5: Arrhenius Plot of the 0-0 peak

A binding energy on this scale is very low compared to most organic semiconductors, suggesting they are highly delocalized, meaning the exciton radius extends over several lattice sites.

Chapter 3

Impedance Spectroscopy of Quinacridone

Metal-semiconductor-metal (MSM) devices with quinacridone as the semiconductor and gold electrodes were characterized by impedance spectroscopy. We found that our devices were well represented by the equivalent circuit model of a resistor and capacitor in parallel. We extracted values for the resistance R and capacitance C of our devices, and for the conductivity (σ) and resistivity (ρ) of quinacridone. The devices showed strong photoconductivity, with the ratio between the light and dark state

$$\frac{\sigma_L}{\sigma_D} = 8.9$$

at room temperature, with a dark conductivity of $\sigma = 1.9110^{-6}[S/(\text{ cm})]$.

3.1 Sample Preparation

In this chapter the MSM devices structures were fabricated on glass substrates, which were washed sequentially in ultrasonic baths of de-ionized water, acetone, and iso-propanol, before cleaning with oxygen plasma. For room temperature measurements, one inch square microscope slides were used, and for low temperature measurement 15 mm square cover slides were used as the substrate. On top of the clean substrate, a 50 nm layer of sublimation gradient purified quinacridone was vapor deposited. The samples were then transferred to a metal evaporator, where a 40 nm layer of gold was evaporated with a source-drain geometry mask. The finished samples mounted in a cryogenic probe station, are shown in Figure 3.1.

3.2 Impedance Spectroscopy

Impedance (Z) is a complex quantity used to characterize the resistance of a device or material to the flow of an AC current. Represented as a vector in the complex plane,

$$Z = R + iX$$

where R is the resistance, and X is reactance. Reactance can be of two kinds, inductive (+) or capacitive (-), but for the devices we are studying, only capacitive reactance (X_c) is observed.

$$X_c = -\frac{1}{2\pi f C}$$

During an impedance spectroscopy measurement, the frequency of the AC signal

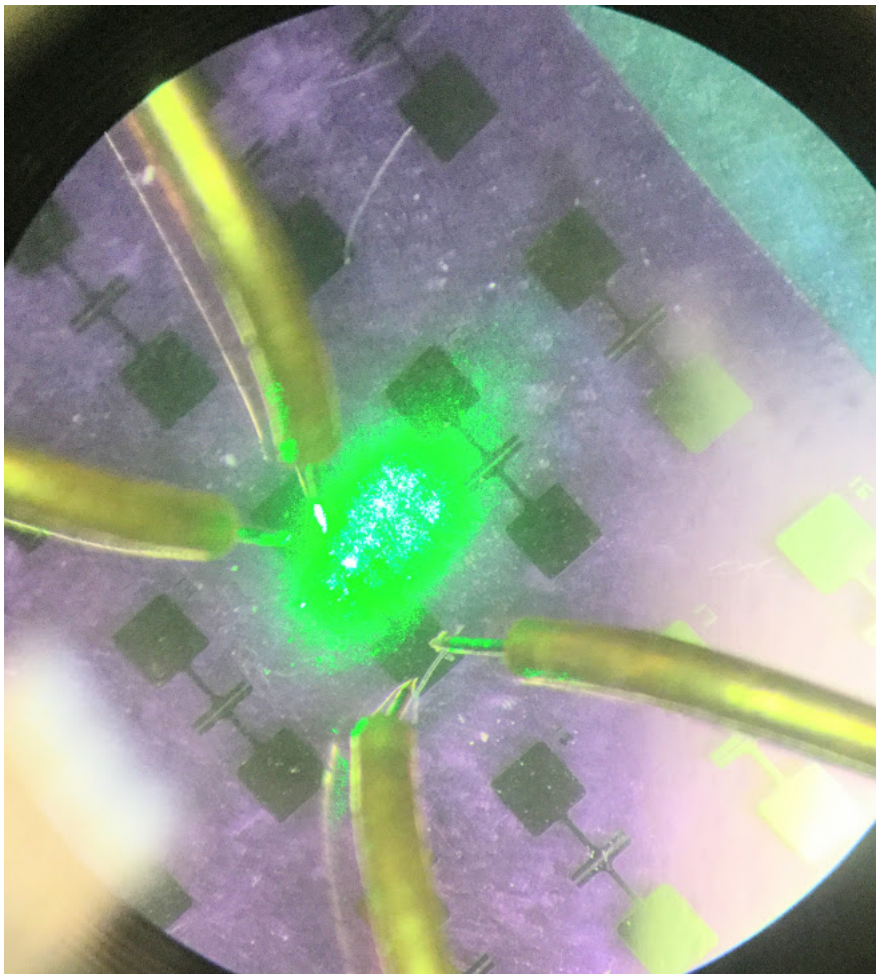

Figure 3.1: Sample Mounted on Probe Station Illuminated with Green Laser for Impedance Spectroscopy Measurement

is varied over eight orders of magnitude, from 10^6 to $10^{-2}Hz$ and measurements of the impedance are taken using a frequency analyzer. In this paper, impedance measurements are shown as Nyquist plots, where the real part of the impedance Z'' is plotted against the imaginary Z'. From this plot we can extract the resistance of the device, which is simply the magnitude of Z' in the low frequency limit, and the capacitance, which is inversely proportional to the max Z''. A Nyquist plot of an ideal resistor and capacitor in series is a semicircle starting from the origin, and terminating on the real axis, at the resistance of the resistor.

3.3 Photoconductivity

Conductivity (σ) is an important material property of an electronic material. Defined as the inverse of the resistivity (ρ)

$$\sigma = 1/\rho = J/E$$

where $\rho = R\frac{A}{L} = R(0.00027)[\Omega]$. In the case of our devices, the resistance, (R), is a function of time since exposure to light. We observe an unexplained, persistent photoconductivity that decays over hours after illumination. The resistance is taken from a semicircular fit of the Nyquist plot, while the device cross-sectional area (A) is

$$A = 1000\mu m \times 0.070\mu m = 70\mu m^2$$

and the length (L) is $26\mu m$, so the ratio $\frac{A}{L} = 0.00027cm^{-1}$.

To measure the effect of light on the MSM device, we exposed the device to a

Table 3.1: Room Temperature Quinacridone Photoconductivity: A Probe Station was used to take measurements, and a green laser was used as an illumination source

	R [Ohm]	C [F]	ρ [Ohm cm]	σ [S/cm]
Light	7.10E+08	9.09E-12	1.91 E+05	5.23 E-06
Dark	1.94E+09	8.50E-12	5.23 E+05	1.91 E-06

bright green laser light source for an hour, before taking a measurement with the light on, which is labeled $t = 1.0$, for the time elapsed in seconds, since the start of the measurement. When this measurement concluded, the light was switched off, and measurements were taken in log-spaced time over 8.3 hours. The resulting Nyquist plot is shown in Figure 3.2. When the light is on, the resistance is almost a factor of 10 times lower than under dark conditions, but it takes many hours for the resistance to relax to an unexcited state.

The decay of the photoconductivity is well modeled by a biexponential function, as shown in Figure 3.3. A fast decay, with a decay lifetime $\tau = 11.7$ minutes, is followed by a slower decay with a decay lifetime $\tau = 2.6$hours.

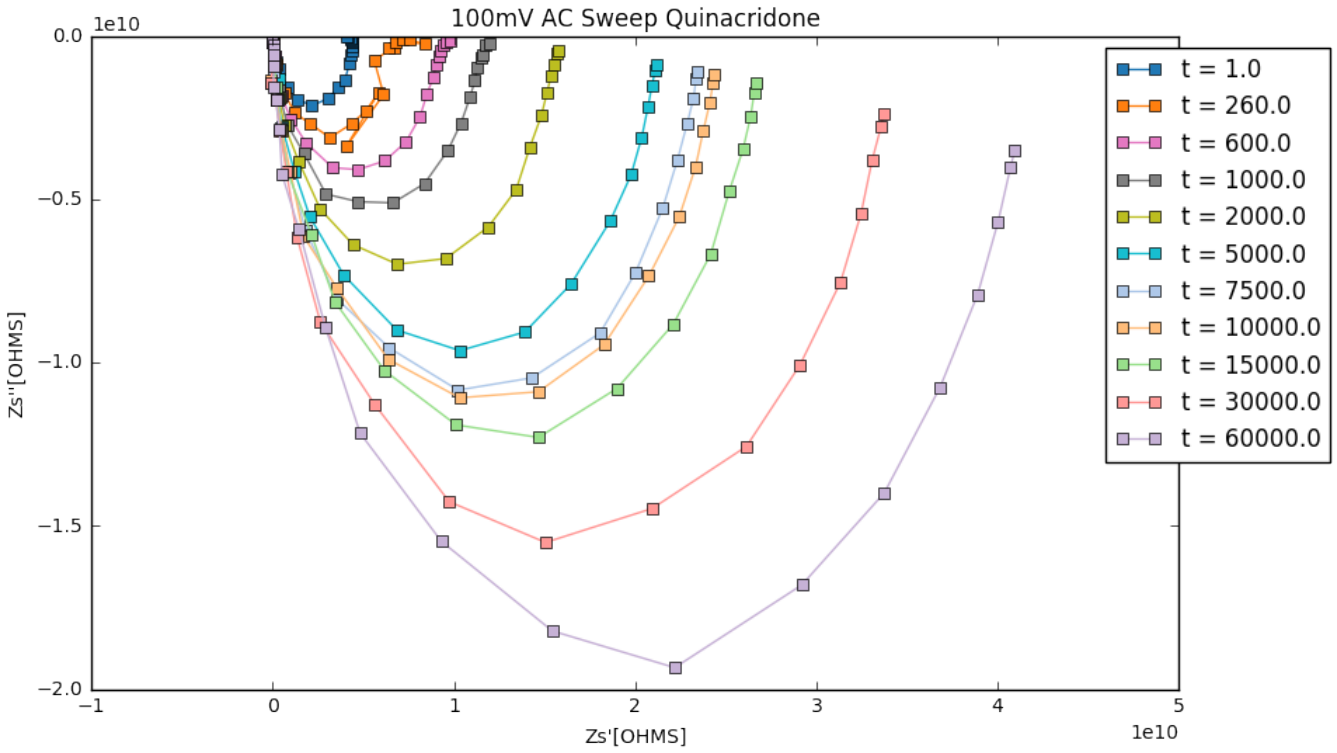

Figure 3.2: Nyquist Plot of Re(Z) vs Im(Z): t=0 denotes the beginning of the measurement, and after one frequency sweep the green LED light source was switched off. The last measurement was taken after more than 16 hours in the dark.

3.4 Temperature Dependence

We examined the temperature dependent photoconductivity in a cyrogenic probe station. The preliminary results are reflected below. As the temperature is lowered, the Nyquist plot in Figure 3.4 shows the resistance of the devices increases substantially, while the capacitance only slightly increases for both light and dark conditions.

Looking at the change in conductivity with temperature, we use the fact that

$$\sigma = qn\mu$$

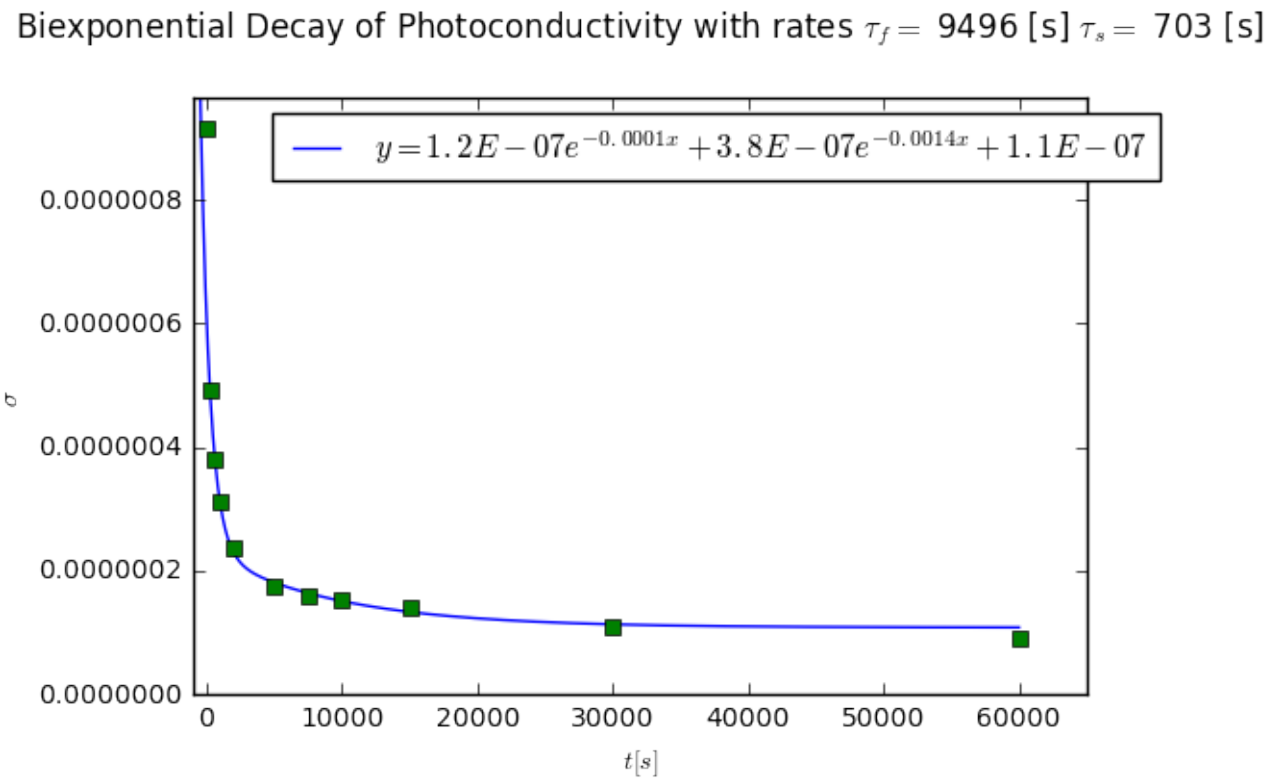

Figure 3.3: Biexponential Decay of Photoconductivity

where q is the electron charge, n is the number of carriers, and μ is the mobility, to fit the conductivity with the thermal generation of carriers[4] [5].

$$\frac{n^2}{n^*} = \kappa \exp \frac{-E_a}{kT}$$

where E_a is the activation energy. The resulting fit shown in Figure 3.5 shows predicted temperature dependence of conductivity, with our measured data. One of the dark data points at 250K was excluded from the fit because it was not allowed to relax fully to the dark state. Unfortunately, the turbo pump on the cryostat probe station was broken after this preliminary data was collected, but even so we see that

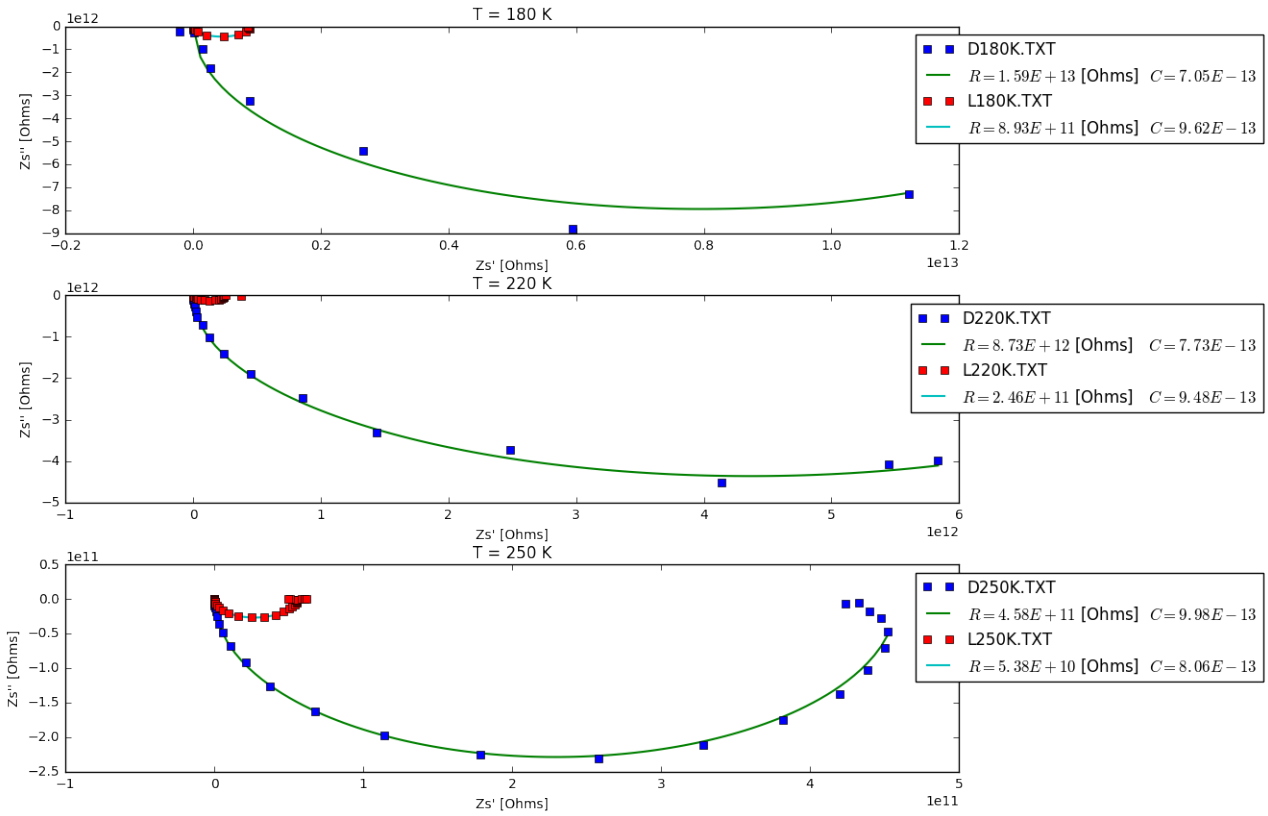

Figure 3.4: Nyquist Plot of Im(Z) vs Re(Z) for low temperatures. Additionally fits for the DC resistance and capacitance have been performed.

the fitted value of the $E_a = 1.4$ meV from our dark conductivity data, which tracks the mobility, and $E_a = 6.4 \pm 0.2$ meV for the light conductivity, which tracks the photo-generated carrier concentration. Subtracting the light activation energy from the dark and doubling gives an estimate of the exciton binding energy[5], which is found to be $E_b = 10 \pm .4$ meV from our measurements. This is on the order of exciton binding energies reported by Glowacki et. al. [6] ($12 \pm 5meV$), and the value obtained from our temperature-dependent PL study (22 meV). While this is comforting, more data points are required to be confident in the results.

By dividing the light conductivity fit by the dark conductivity fit, we obtain an approximation of the temperature dependence of the on/off ratio, as shown in Figure 3.6. We see that for high temperatures, the ratio between light and dark conductivity is high, but that as fewer charges are thermally excited at low temperatures, we expect a decrease in the proportion of free charge carriers generated from photo-excitation.

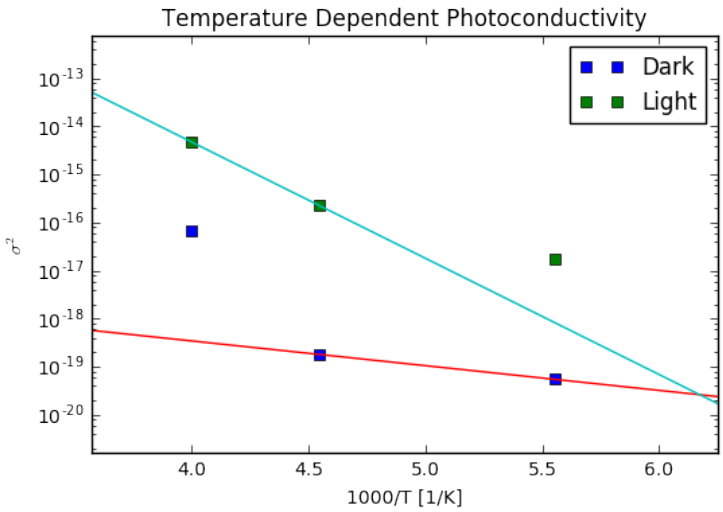

Figure 3.5: Temperature Dependence of Photoconductivity

Most of the measurements taken were too noisy to extract a meaningful resistance, which could be a result of inconsistent times for relaxation to the dark state after illumination, imperfect contact between the probes and the top metal electrode, the lack of a true dark environment for dark measurements, or the destruction of the sample as the probe tips were moved without the use of a camera in the cryostat.

Ideally, additional low temperature studies would be undertaken, where the light and dark measurement would be measured after at least two half lives of the fast decay at each temperature point. Also a full 10 hour decay at 100 K would be interesting to see if slow rate of decay is temperature dependent.

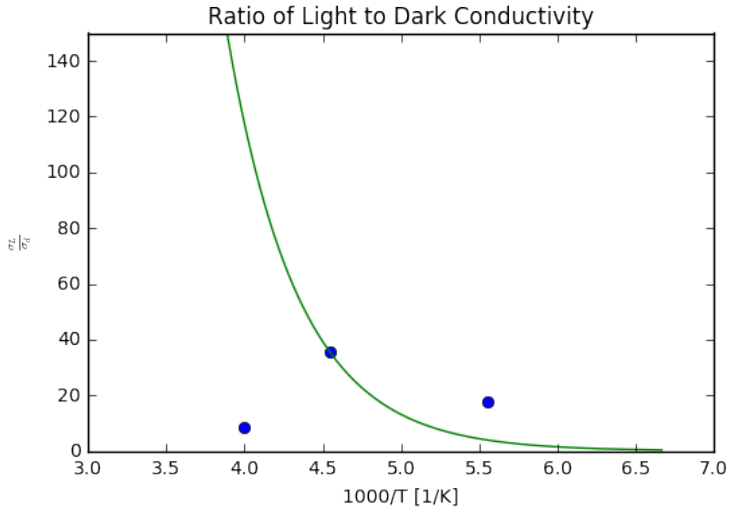

Figure 3.6: Ratio of light and dark conductivity fits

Chapter 4

Diodes

4.1 Sample Preparation

In order to fabricate diode samples, pre-patterned Indium Tin Oxide (ITO) substrates were washed sequentially in ultrasonic baths of de-ionized water, acetone, and iso-propanol, before cleaning with oxygen plasma. Next, the samples were spin coated with Poly(3,4-ethylenedioxythiophene) (PEDOT) with two layers spinning at 4000 rpm for 45 seconds. The edges were wiped clean to expose the ITO contact pads. A 80 ± 10nm layer of sublimation gradient purified quinacridone was vapor deposited over the PEDOT layer. Finally at 150 nm layer of aluminum was vapor deposited as the top contact. A completed sample mounted on a Solar Simulator is shown in Figure 4.1. Cells were tested within one hour of being exposed to air, as the performance was degraded as the aluminum top contacts were oxidized.

4.2 Current - Voltage [IV] Curves

To evaluate the quality of quinacridone as semiconductor for diode devices, the current driven through the system was measured as a function of voltage under light and dark conditions to examine their photoresponse. To measure the devices, they were mounted on the sample holder pictures in Figure 4.1, which was connected to a Keithley 2401 source meter which measured the current at a series of voltages from -1 V to 2 V.

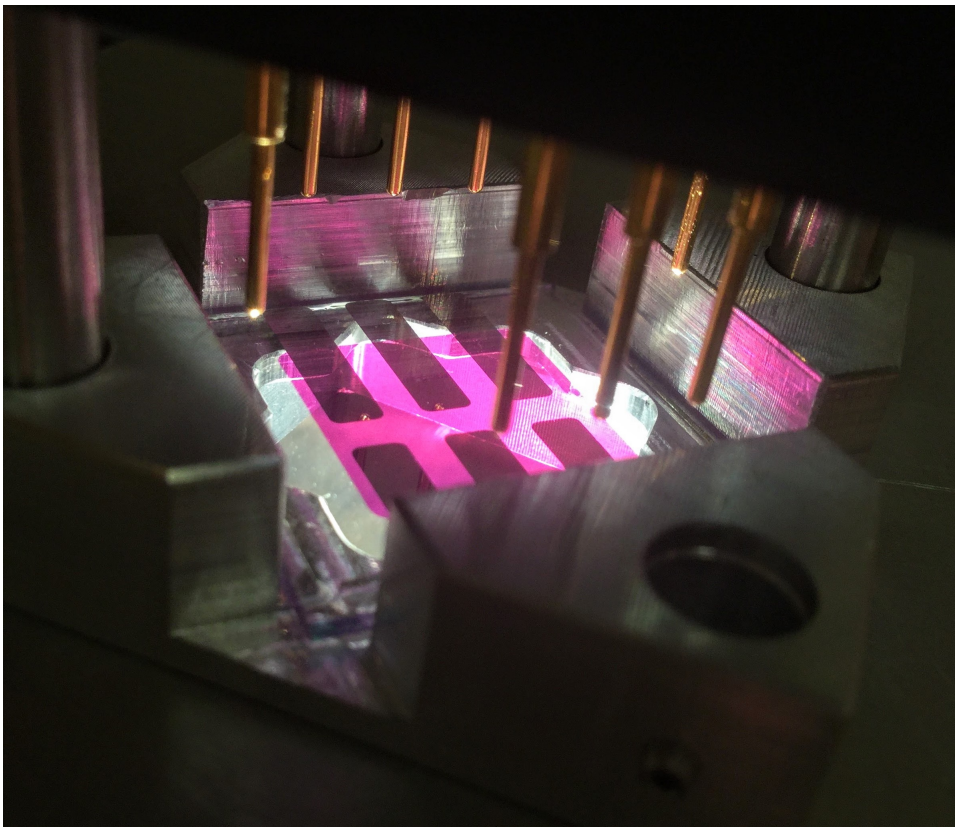

Figure 4.1: Quinacridone Diode Mounted on Solar Simulator

The resulting IV curves are reflected below in Figure 4.2.

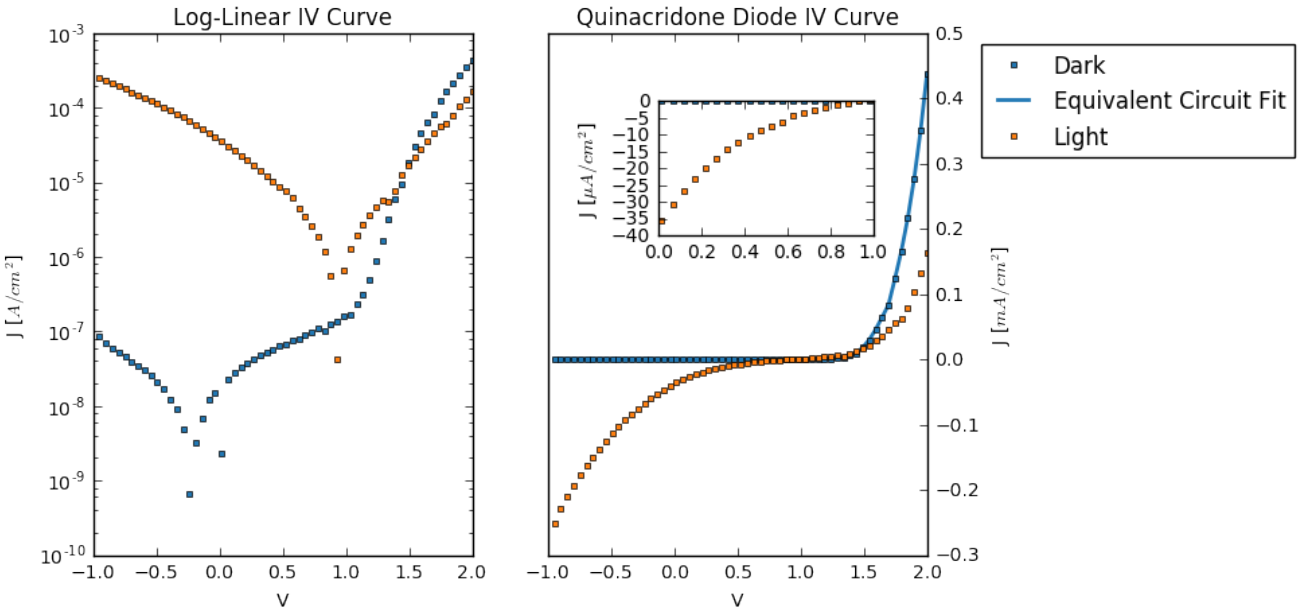

Figure 4.2: Quinacridone Diode IV Response: Light and Dark
Inset shows $I_{sc} \approx 37$ [μA] and $V_{OC} \approx 0.9$ [V]

We can clearly see the difference between the IV curves under light and dark conditions. The dark curve has a characteristic diode curve, where no current flows in reverse bias, when the applied voltage is negative, and an exponential increase in current as the applied voltage increases in forward bias. The light curve is offset by the photocurrent generated, but it is much lower than expected from previous reports, which found $J_{SC} = 1mA/cm^2$ under light conditions using an identical device structure[6]. We observed $J_{SC} = 20\mu A/cm^2$, 50 times smaller than the previously reported value.

A fit of the diode based on the equivalent circuit model where the total current generated (I_{tot}) is a sum of three component currents, light generated current (I_L), diode current (I_D), and shunt current (I_{sh}), where the latter two have a negative sign

since they represent current lost to recombination in the diode or to shunt resistances. Thus the modeling equation for the total current is given by

$$I = I_L - I_D - I_{sh}$$

$$I = I_L - I_0\left(\exp\left(\frac{V + IR_s}{nV_T} - \right)1\right) - \frac{V + IR_s}{R_{sh}}$$

where V and I are the applied voltages and observed currents, V_T is the thermal voltage, n is the ideality factor of the diode, R_s is the series resistance, and R_{sh} is the shunt resistance [7]. The fitted values are shown in Table 4.1. We see the series resistance is about 280 Ohms, higher than ideal for a well functioning solar cell, likely because our fabrication and testing of the device in ambient air allows AlO_x to form on the diode's Al top electrodes.

Table 4.1: Fitted Equivalent Circuit Parameters for Diode Under Dark Conditions

I_L	I_0	n	R_s	R_{sh}
(-5.8 ± 4) e-08	(-3.3 $\pm$0.9) e-11	(5.018 $\pm$ 0.1) e+00	(1.84 $\pm$ 0.07) e+03	(7.6 $\pm$ 300) e+08

4.3 Transient Photovoltage

In addition to the series resistance, some other factors may be inhibiting the extraction of photocurrent from the diode under light conditions. Charge transfer states could be recombining before they can be extracted from the diode as free charge carriers. To understand how long excited CT states survive before recombination, we performed a transient photovoltage measurement, which examines how the voltage decays under short circuit conditions when the incident intensity of light is varied.

To take this measurement a Tektronics MDO3024 oscilloscope was used to measure the diode voltage as a function of time, as well as the current powering a square wave modulated LED light source operating at 30 Hz. The amplitude of the square wave was restricted to less than 10% of the overall current powering the LED. The intensity of the resulting decay, shown in Figure 4.3, is well modeled as a single exponential,

$$\Delta V(t) \propto \exp(t/-\tau)$$

since the amplitude is within the small perturbation regime of the total offset [8], with a carrier lifetime of $\tau = 630 \pm 5\ \mu$s.

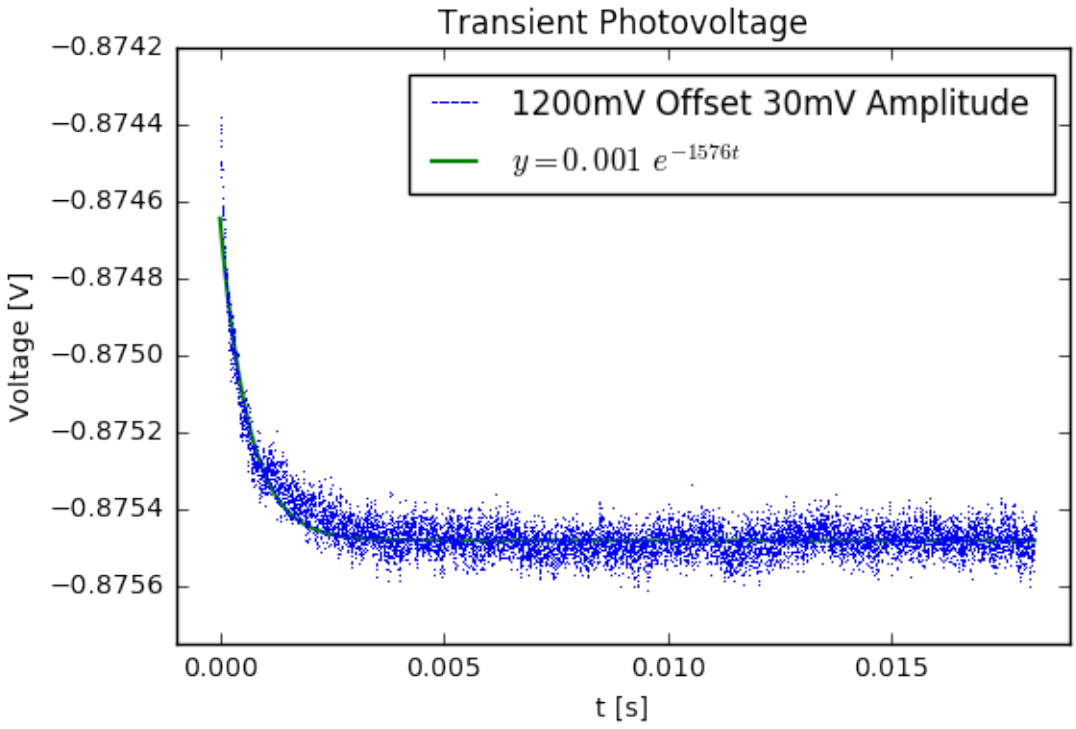

Figure 4.3: Quinacridone Photovoltage

4.4 Photocurrent

To better understand the dynamic behavior of charge carriers within the quinacridone diode, a transient photocurrent measurement was conducted, using the same oscilloscope and LED light source as above, but with an amplifier to magnify the weak light generated current. A square wave with a 600mV offset and 100 mV amplitude was used to drive the LED operating at 100 Hz. The resulting data, shown in Figure 4.4 was fitted with an exponential and then a biexponential fit, when the former was found to be inadequate, indicating that there are two different timescales. This is most likely caused by a mismatch between electron and hole mobility within the device, but could also be the result of charge carriers being generated predominately adjacent to the ITO electrode, the side through which light enters and is absorbed. From this biexponential fit, we found that the fast process had a constant of $\tau_f = 0.0000038s = 3.8 \pm 0.2\mu s$ and the slow process had a time constant of $\tau_s = 0.0000321s = 32 \pm 4\mu s$.

Another possible explanation for the need for a biexponential with the slow process corresponding to trapping, and the fast process corresponding to the steady state mobility [9].

Comparing the two extraction time constants of $\tau_f = 3.8 \pm 0.2\mu s$ and $\tau_s = 32 \pm 4\mu s$ to the CT state lifetime $\tau = 630 \pm 5\mu s$, we see that the timescale on which charge extraction would occur under operating conditions is at least an order of magnitude smaller than the CT state lifetime. Thus CT state lifetime is not limiting the current generation of these devices for solar energy applications, as the time is takes charges to move through the diode is much smaller than the time it takes to recombine. Rather

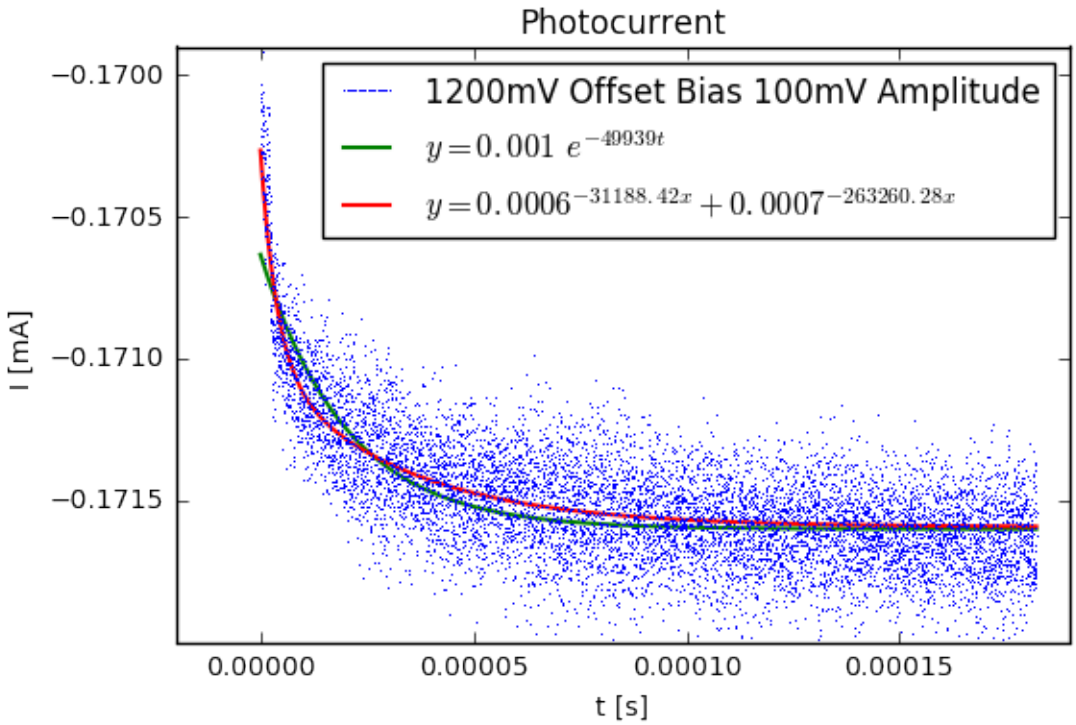

Figure 4.4: Quinacridone Photocurrent

the free charge carrier generation, which is controlled by the probability of exciton dissociation, likely reduces the current to below usable levels.

4.5 Onsager Braun Theory

The light curve is not well fit by the simplistic ideal diode model because not all of the charge transfer states generated by the incident photons dissociate into free charges. Rather the probability of dissociation is dependent on applied field as described by Braun [10], who adapted Onsager's [11] [12] work on bound ion dissociation in solution, to the dissociation of charge transfer states into free carriers in semiconductors:

$$P(E) = \frac{k_d(E)}{k_d + k_f}$$

where $k_d(E)$ is the electric field dependent rate of dissociation, and k_f is the constant rate of exciton relaxation to the ground state. For organic systems where the charge transfer excition (CT) state is sufficiently localized, we can approximate the state as classical ion pairs, leading to a electric field dependent rate of dissociation:

$$k_d(E) = ve^{-\Delta E/k_bT} J_1[2\sqrt{-2b}]/\sqrt{-2b} = ve^{-\Delta E/k_bT}\left(1 + b + b^2/3 + b^3/18\ldots\right)$$

where J_1 is a first order Bessel function, in order to satisfy the cylindrical boundary conditions placed on the divergence-less ion flux in Onsager's analysis [12], $b = e^3E/(8\pi\langle\epsilon\rangle\epsilon_0 k^2T^2$, ΔE is the exciton binding energy, and

$$v = \frac{3\langle\mu\rangle e}{4\pi\langle\epsilon\rangle\epsilon_0 a^3}$$

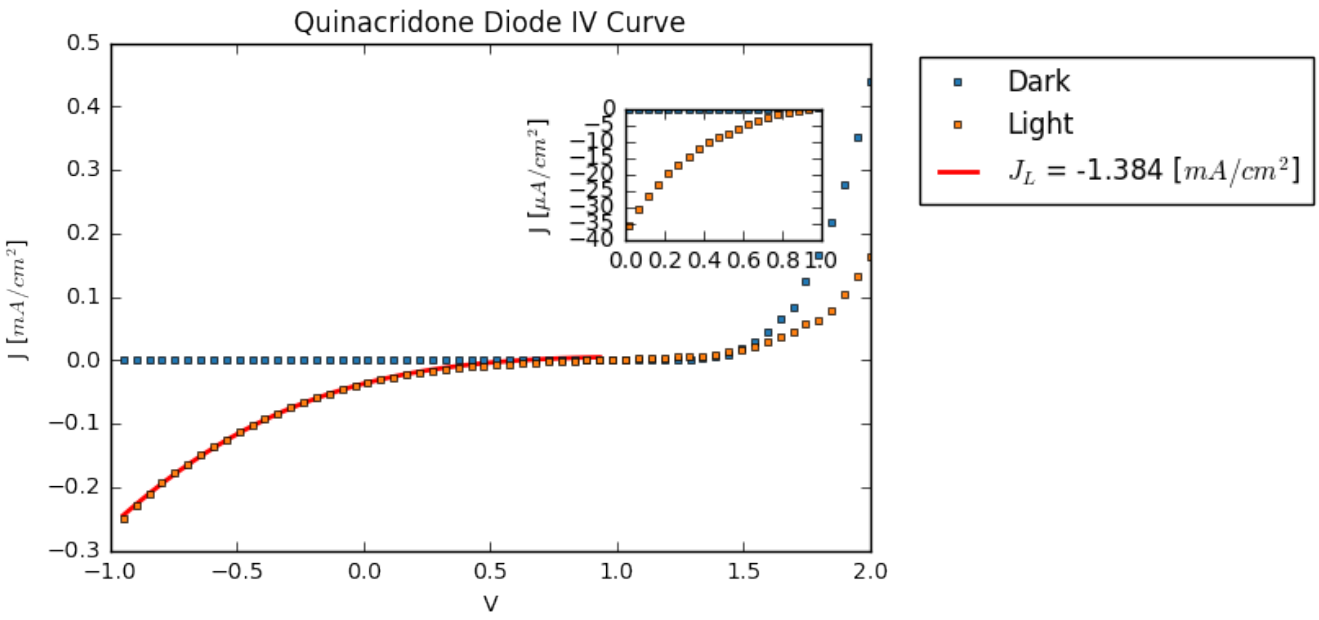

Figure 4.5: Quinacridone Diode IV Response: Light and Dark
Inset shows $I_{sc} \approx 37$ [μA] and $V_{OC} \approx 0.9$ [V]

for a classical ion pair, where μ is the mobility, $\langle\epsilon\rangle$ is the dielectric constant. The values used are list in Table 4.2 were taken from published values from Glowacki et al [6], while the dissociation and relaxation rates ($k_d(0)$, k_f), were calculated from these values.

Table 4.2: Onsager Braun Parameters

$\langle\mu\rangle$ [cm^2/s]	ΔE [meV]	k_BT[meV]	ϵ [F/m]	k_f [1/s]	$k_d(0)$ [1/s]
0.001	12	25.7	4.2	10^8	2.76 $\times 10^6$

While fitting for the maximum light current I_L in Figure 4.5, we obtain a very good fit for the quinacridone diode under light conditions, where the fit is valid over the range where the internal field of the diode is negative, from -1 to 1 V externally applied voltage. The fitted light current $J_L = 1.3$ is on the same order as the reported

value of J_{SC} for PEDOT - quinacridone diodes reported by Glowacki et al. [6].

If the mobility of carriers in the quinacridone could be increased, by controlling the rate of deposition and the temperature of the substrate in order to increase the crystalline order of the quinacridone semiconducting layer, we would see a significantly higher probability of exciton dissociation ($P(E)$), even at zero applied field. Additionally, controlling the fabrication environment to eliminate the formation of AlO_x would create a higher "built-in" electric field, further increasing P(E), and thus increasing J_{SC} to or above the levels previously reported.

Chapter 5

Conclusions and Future Work

A number of thin-film samples and device structures were characterized by a suite of optical and electronic tests. Optical tests on vapor-deposited quinacridone thin films confirmed that quinacridone absorbs over a relatively broad range of visible wavelengths, and absorbed light produces an exciton of binding energy 22 $\pm$ 1.2 meV, which suggests delocalization over several lattice sites. In order to investigate the exciton dynamics further, it would be interesting to measure the exciton diffusion length by running a thickness-dependent photoluminescence quenching experiment, where the internal field is held at zero at each thickness to inhibit exciton dissociation into free carriers. Then as the thickness of the quinacridone layer increases, we should see an increase in photoluminescence, as the distance from the acceptor layer to the bulk of exciton photo-generation exceeds the exciton diffusion length.

Electronic tests showed that quinacridone had a conductivity of $\sigma = 1.9 \times 10^{-6}$[S/cm], and found a thermal activation energy for the photo-generation of charge carriers. However, we hope to run further temperature-dependent impedance spectroscopy tests once our turbo-pump is fixed to give a more convincing temperature

dependent dataset.

Finally, by testing an ITO:PEDOT:Quinacridone:Al diode device, we were able to show that device performance is not limited by free carrier lifetimes, which were found to have lifetimes of $\tau = 630 \pm 5\mu s$, far longer than the extraction time constants of $\tau_f = 3.8 \pm 0.2\mu s$ and $\tau_s = 32 \pm 4\mu s$. Rather the lack of exciton dissociation, which is inhibited by the low mobility of our polycrystalline thin-films, limits the current generation, and our weighting of the light current by the probability of exciton dissociation is a satisfactory model to explain the deviation from the expected ideal diode IV characteristic lineshape.

Bibliography

[1] S. Yoo, B. Domercq, and B. Kippelen, "Efficient thin-film organic solar cells based on pentacene/c60 heterojunctions," Applied Physics Letters **85**, 5427 (2004), http://dx.doi.org/10.1063/1.1829777 .

[2] E. D. Głowacki, L. Leonat, M. Irimia-Vladu, R. Schwödiauer, M. Ullah, H. Sitter, S. Bauer, and N. S. Sariciftci, "Intermolecular hydrogen-bonded organic semiconductors—quinacridone versus pentacene," Applied Physics Letters **101**, 023305 (2012), http://dx.doi.org/10.1063/1.4736579 .

[3] M. Kasha, H. R. Rawls, and M. Ashraf El-Bayoumi, "The exciton model in molecular spectroscopy," Pure and Applied Chemistry **11** (1965).

[4] R. O. Loutfy, "Effect of temperature on the dark and photoconductivity of metal-free phthalocyanine," physica status solidi (a) **65**, 659 (1981).

[5] G. Horowitz, F. Kouki, P. Valat, P. Delannoy, and J. Roussel, "Photoconductivity of sexithiophene single crystals," Physical Review B **59**, 10651 (1999).

[6] E. D. Głowacki, L. Leonat, M. Irimia-Vladu, R. Schwödiauer, M. Ullah, H. Sitter, S. Bauer, and N. S. Sariciftci, "Intermolecular hydrogen-bonded organic

semiconductors—Quinacridone versus pentacene," Applied Physics Letters **101**, 023305 (2012).

[7] J. L. Gray, "The physics of the solar cell," *Handbook of Photovoltaic Science and Engineering*, , 61 (2005).

[8] C. G. Shuttle, B. O'Regan, A. M. Ballantyne, J. Nelson, D. D. C. Bradley, J. de Mello, and J. R. Durrant, "Experimental determination of the rate law for charge carrier decay in a polythiophene: Fullerene solar cell," Applied Physics Letters **92**, 093311 (2008).

[9] C. R. McNeill, I. Hwang, and N. C. Greenham, "Photocurrent transients in all-polymer solar cells: Trapping and detrapping effects," Journal of Applied Physics **106**, 024507 (2009).

[10] C. L. Braun, "Electric field assisted dissociation of charge transfer states as a mechanism of photocarrier production," The Journal of Chemical Physics **80**, 4157 (1984).

[11] L. Onsager, "Initial Recombination of Ions," Physical Review **54**, 554 (1938).

[12] L. Onsager, "Deviations from Ohm's Law in Weak Electrolytes," The Journal of Chemical Physics **2**, 599 (2004).